ARTICLE

Adaptive learned iterative shrinkage-thresholding algorithm combined with a physics-driven self-supervised method for sparse spike deconvolution

Shunhao Hu[1,2], **Shulin Pan[1]***, **Ziyu Qin[1,3]**, **Yinghe Wu[4]***, and **Yaojie Chen[2]**

[1]State Key Laboratory of Oil and Gas Reservoir Geology and Exploitation, Southwest Petroleum University, Chengdu, Sichuan, China

[2]Reservoir Geophysical Laboratory, School of Geoscience and Technology, Southwest Petroleum University, Chengdu, Sichuan, China

[3]Department of Software Engineering, School of Computer Engineering, Chengdu Technological University, Chengdu, Sichuan, China

[4]State Key Laboratory of Lithospheric Evolution, Institute of Geology and Geophysics, Chinese Academy of Sciences, Beijing, China

Abstract

The conventional iterative shrinkage-thresholding algorithm (ISTA) faces several limitations, such as dependence on manual parameter tuning and limited ability to recover weak reflections. Hence, this study proposes a sparse spike deconvolution method based on an adaptive learned ISTA (Ada-LISTA) and a self-supervised physics-driven objective function to overcome these challenges. First, using Ada-LISTA as the backbone, the threshold and step size in the iterative process were dynamically adjusted through its adaptive parameter learning, and the seismic wavelet dictionary was used as the model input to enhance the adaptability to different complex geological scenarios. Then, a self-supervised physics-driven objective function was introduced to jointly optimize the residual of seismic records and the sparsity of reflection coefficients, further improving the interpretability of the model. Finally, comparative experiments were carried out using theoretical simulation data and actual seismic data from the Bohai Bay Basin, China, to evaluate the inversion performance of the proposed method. The experimental results indicate that, compared to the traditional ISTA algorithm, the proposed method achieved marked enhancements in reflection coefficient inversion accuracy, seismic resolution, and robustness against noise. Overall, the proposed method offers an efficient and reliable technical solution for high-resolution seismic inversion and effective recovery of weak reflection signals, providing practical support for interpreting complex subsurface geological structures.

Keywords: Sparse spike deconvolution; Seismic resolution; Weak reflection; Adaptive learned iterative shrinkage-thresholding algorithm; Physics-driven self-supervised method

1. Introduction

Sparse spike deconvolution, which inverts the underground reflection coefficient sequence using seismic records with limited bandwidth, is a common processing approach to enhance seismic data resolution.[1] The spectral sparse reconstruction proposed by Levy and Fullagar[2] and the two-dimensional Bayesian inversion framework by Lavielle[3] have collectively laid the foundation for the theoretical development of sparse spike deconvolution. Studies of well-log data have shown that primary reflection coefficients typically exhibit spectral non-whiteness[4] and amplitude distributions that are distinctly non-Gaussian, which fundamentally influence the design of effective deconvolution methods.[5] Based on these observations, the core principle of sparse spike deconvolution is to formulate seismic inversion as a linear inverse problem in which the reflectivity is modeled as a sparse impulse sequence and L1 regularization is used to promote sparsity.[6] The solution methods can be categorized into two groups, namely convex optimization methods founded based on pursuit[7] and greedy iterative algorithms derived from matching pursuit.[8,9] Among these, the iterative shrinkage-thresholding algorithm (ISTA) introduced by Beck and Teboulle[10] converts the non-smooth L1 regularization problem into an iteratively solvable optimization problem by introducing a soft-thresholding operator, thus becoming a widely used standard numerical solution in the field of sparse spike deconvolution. However, the traditional ISTA algorithm exhibits numerous limitations in practical applications. Specifically, its threshold and step size parameters rely heavily on manual adjustment.[11] Moreover, it is highly sensitive to the initial dictionary,[12] struggles to process complex seismic data,[13] and performs poorly in recovering weak reflection coefficients.[14]

To overcome these limitations, researchers have started to develop novel algorithmic frameworks using deep learning techniques.[15-17] In contrast to traditional methods that rely on manually designed iterative rules, these new approaches enable algorithms to automatically learn efficient solution strategies in a data-driven manner.[18] Gregor and LeCun[19] developed the learned ISTA (LISTA) by unfolding the iterative process of ISTA into a neural network structure, enabling end-to-end learning of parameters to adapt to signal distributions, accelerate convergence, and achieve automatic parameter optimization. Inspired by this, researchers have conducted extensive explorations on deep learnable sparse solver methods in fields such as seismic exploration and high-resolution imaging. In recent years, focusing on LISTA and its iteratively unfolded networks, researchers have proposed various variants. Analytic LISTA[20] adopts analytical parameters to simplify

training while ensuring theoretical convergence. Gated LISTA[21] introduces gating and compensation mechanisms to enhance the expressive ability in adjusting sparse components and step sizes. Hybrid LISTA[22] realizes a more flexible network structure design through a hybrid form of iterative unfolding architecture. Step-LISTA[23] achieves step size learning to accelerate convergence. Extragradient-based LISTA[24] enhances the network recovery performance through residual structures and improved threshold functions. LISTA with adaptive thresholds[25] employs element-wise adaptive thresholds to improve the algorithm's adaptability to different sparse signals. Extragradient analytic LISTA and fast analytic LISTA,[26] respectively, enhance the robustness and accuracy of inversion under limited observations by introducing residual connections and momentum acceleration. LISTA with coupled weights and support selection[27] optimizes convergence efficiency through a support selection structure. Adaptive threshold analytic LISTA-based sparse imaging network[28] has shown excellent performance in high-resolution imaging tasks such as high-resolution synthetic aperture radar tomography and three-dimensional reconstruction, effectively improving spatial resolution under limited observation conditions. These methods have made significant progress in parameter adaptability, convergence speed, and complex signal expression, but they still rely on fixed dictionaries, making it difficult to adapt to complex environments. To address this limitation, Aberdam *et al.*[29] developed the adaptive LISTA (Ada-LISTA), which improves the model's adaptability to different scenarios by taking the dictionary as input. However, Ada-LISTA currently mainly targets general signal processing tasks and adopts a supervised learning approach, which has high demands on prior labels. It has not yet been effectively applied in the field of geophysics, especially in the recovery of weak reflection signals.

The traditional ISTA, which relies on global static thresholds and fixed dictionaries, frequently results in excessive suppression of low-amplitude reflection coefficients and consequently impedes the effective recovery of weak signals. Meanwhile, although supervised learning models perform excellently under ideal label conditions, the number of on-site logging labels is limited,[30] resulting in insufficient generalization performance.[31] In recent years, unsupervised and semi-supervised frameworks have gradually become new trends in seismic inversion.[32] On one hand, researchers have widely incorporated physical constraints, such as the seismic wave equation[33] and forward modeling,[34] constructed physically consistent losses,[35] and trained networks in an unsupervised manner to achieve effective recovery of weak seismic reflections and high-resolution structural information.[36] On the other

hand, they have adopted semi-supervised and multi-task learning frameworks, combined attention mechanisms[37] to enhance the feature expression of high-frequency and weak components, employed domain-adaptive adversarial training[38] to effectively improve the generalization ability of models to complex structures and unknown environments, and introduced amplitude versus angle physical priors[39] to strengthen the physical consistency and interpretability of models. These measures have significantly alleviated the generalization bottleneck caused by scarce labels in seismic inversion[40] and achieved remarkable improvements in the identification of complex seismic records and thin-layer weak reflection signals.[41] These research advances verify the advantages of physics-driven unsupervised methods and provide an important basis for the construction of the objective function in this study.

Given the limitations of the traditional ISTA algorithm in recovering weak reflection signals and the reliance of existing learning-based methods on fixed dictionaries and labeled data, this study proposes a self-supervised Ada-LISTA-based sparse inversion method for weak reflection signals. Through a hierarchical iterative optimization structure, adaptive learning of parameters and dynamic adaptation of the dictionary are achieved. The physics-driven self-supervised method is employed to ensure that inversion results conform to geophysical laws, and seismic record reconstruction is performed. The proposed method is tested using theoretical model data and actual oilfield data.

2. Methodology

2.1. ISTA

Under the assumptions of the convolutional model in seismic exploration, $y(t)$ let y denote the seismic record, $d(t)$ denote the seismic wavelet and $x(t)$ denote the reflection coefficient. The relationship among the three can be expressed as **Equation 1**:

$$y(t) = d(t) * x(t) + n(t) \tag{1}$$

where $n(t)$ is random noise.

Based on **Equation 1**, sparse spike deconvolution can be expressed as **Equation 2**:

$$\underset{x}{\mathrm{argmin}}\left(\frac{1}{2}Dx - y_2^2 + \lambda x_1\right) \tag{2}$$

Where y is the seismic record vector, D denotes the dictionary composed of seismic wavelets, x denotes the reflection coefficient vector to be solved, λ is the regularization parameter, $\left\|\cdot\right\|_2^2$ denotes the square of the

Euclidean norm, and $\left\|x\right\|_1$ is the sum of the absolute values of all components of x.

Equation 2 can be solved using the ISTA algorithm,[10] and the result is expressed as **Equation 3**:

$$x_{k+1} = S_\theta\left(x_k - \frac{1}{L}D^T\left(Dx_k - y\right)\right) \tag{3}$$

Where D^T is the transpose matrix of D, L ($L>0$) is the Lipschitz constant, $\gamma = 1/L$ is the step size parameter, x_{k+1} and x_k are the optimal reflection coefficients of the k+1-th and k-th iterations, respectively, θ is the threshold, and S_θ (p) is the soft thresholding function, defined as **Equation 4**:

$$S_\theta\left(p\right) = \begin{cases} p+\theta, & p \le -\theta \\ 0, & |p| < \theta \\ p-\theta, & p \ge \theta \end{cases} \tag{4}$$

Let $U = \frac{1}{L}D^T$, $H = I - \frac{1}{L}D^TD$, and I be identity matrices, then **Equation 3** can be simplified as **Equation 5**:

$$x_{k+1} = S_\theta\left(Uy + Hx_k\right) \tag{5}$$

The iterative flow chart of ISTA is shown in Figure 1. In actual calculations, both threshold θ and step size parameter γ need to be set manually. In the actual experimental process, it is necessary to repeatedly try different values to optimize the results. In addition, ISTA relies on a fixed threshold, and weak reflection coefficients are prone to excessive compression.

2.2. LISTA

To simplify the cumbersome parameter tuning problem caused by fixed parameters in ISTA, Gregor and LeCun[19] developed the LISTA. Its core is to reconstruct the iterative process of ISTA into a deep neural network architecture. The k-th iteration of ISTA corresponds to the k-th layer of the network, and the iteration formula for each layer is expressed as **Equation 6**:

$$x_{k+1} = S_{\theta_k}\left(U_k y + H_k x_k\right), k = 0,1,\cdots,k-1 \tag{6}$$
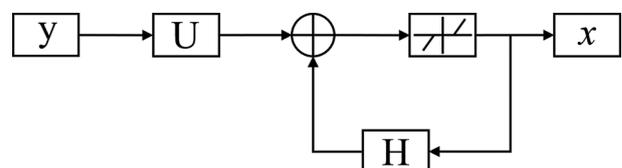

Figure 1. The iterative shrinkage-thresholding algorithm architecture

Where θ_k is the learnable threshold parameter of the k-th layer, and U_k and H_k are learnable matrices of the k-th layer.

During initialization, $U_k = \frac{1}{L}D^T$, and $H_k = I - \frac{1}{L}D^T D$.

Figure 2 shows the network architecture of LISTA. The seismic record y is multiplied by matrix U, then added to Hx, and processed by a soft-thresholding function. This result serves as the input to the next layer, and the process is repeated. After multi-layer cascaded operations, the reflection coefficient x is finally obtained.

A comparison of Figures 1 and 2 reveals a clear structural connection between ISTA and LISTA. Each iteration in ISTA can be regarded as a network layer in LISTA. The input and output of each layer are computed using learnable matrices and thresholds. Unlike ISTA, the parameters of each layer in LISTA are automatically adjusted based on data during training without manual setting. Through an end-to-end learning approach, LISTA converts the ISTA algorithm into a trainable network structure, thereby improving the recovery performance of reflection coefficients.

2.3. Ada-LISTA

Although LISTA significantly optimizes the training process of ISTA through learnable parameters, it is still limited by its reliance on a fixed dictionary during the training phase. Due to the lack of dynamic adaptability in the fixed dictionary, it is difficult to accurately identify reflection signals with weak energy and sparse features. Such signals are easily misjudged as noise and incorrectly suppressed.

To break through this bottleneck, this study introduces the Ada-LISTA[29] framework proposed by Aberdam *et al.*[29] This framework is improved based on LISTA. It not only takes the dictionary as the model input, but also introduces two auxiliary weight matrices W and M, enabling the model to dynamically adjust parameters according to different signals and dictionaries, thereby enhancing the flexibility of inference.

Specifically, the Ada-LISTA iteration formula is defined as **Equation 7**:

$$x_{k+1} = S_{\theta_k}\left(\left(I - \gamma_k D^T W_k^T W_k D\right)x_k + \gamma_k D^T M_k^T y\right) \qquad (7)$$

Where θ_k, γ_k, W_k, and M_k are learnable parameters, θ_k is the threshold parameter of the k-th layer, γ_k is the step size parameter of the k-th layer, $W_k, M_k \in \mathbb{R}^{n \times n}$ is an auxiliary weight matrix, I is the identity matrix.

A comparison of **Equations 3**, **5**, **6**, and **7** shows that ISTA, LISTA, and Ada-LISTA present an obvious progressive relationship in structure. ISTA (**Equations 3** and **5**) adopts fixed parameter matrices U and H to solve input signals iteratively. Its parameters need to be manually specified, making it difficult to adapt to the characteristics of different signals. LISTA (**Equation 6**) unfolds the iterative process of ISTA into a multi-layer network structure and treats U and H as learnable parameter matrices. It realizes automatic parameter adjustment through adaptive optimization with training data. Ada-LISTA (**Equation 7**) further refines the parameter structure and uses weight matrices W and M to construct the original U and H more elaborately. It adjusts $U_k = \frac{1}{L}D^T = \gamma_k D^T$ in LISTA to $\gamma_k D^T M_k^T$ through M in Ada-LISTA, and adjust $H_k = I - \frac{1}{L}D^T D = I - \gamma_k D^T D$ to $I - \gamma_k D^T W_k^T W_k D$ through W. This enables each layer to fine-tune the dictionary via weight matrices W and M, enhancing adaptability to different seismic data. In general, these three methods gradually improve in parameter expression, structural setting, and adaptability, fully reflecting the development process of the model from fixed parameters to learnable parameters and then to dynamically adaptive parameters.

As shown in Figure 3, Ada-LISTA further extends the design of LISTA in the network structure. By introducing weight matrices W and M, Ada-LISTA can achieve hierarchical adaptive adjustment of input signals and dictionary information. Compared with LISTA, Ada-LISTA maintains the benefit of learnable parameters while improving adaptability to varying seismic data conditions through dynamic dictionary adjustments. This structure
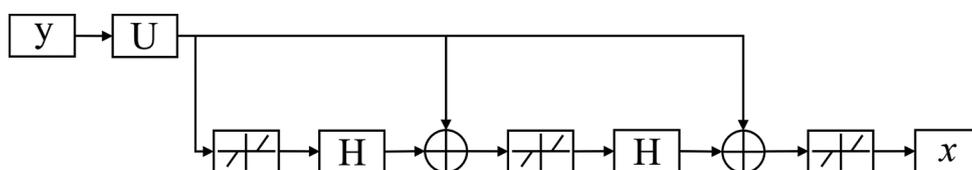
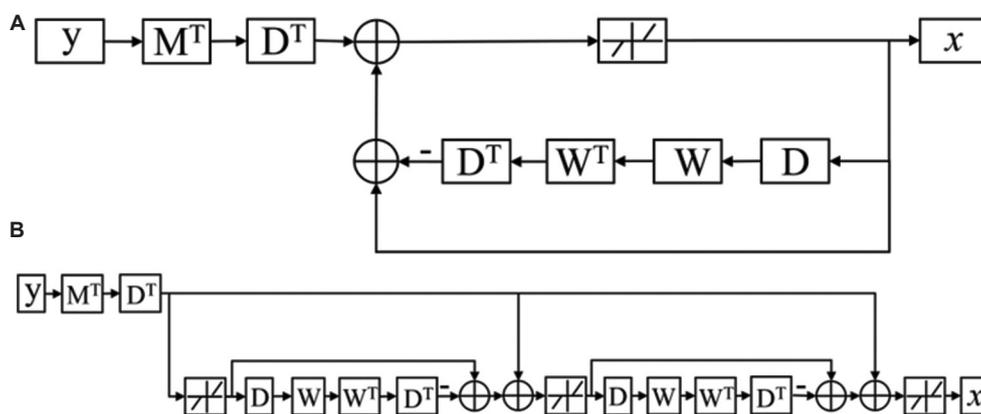**Figure 2.** The learned iterative shrinkage-thresholding algorithm architecture

Figure 3. Adaptive learned iterative shrinkage-thresholding algorithm architecture. (A) Iterative model. (B) Unfolded model.

effectively improves the ability to identify weak reflection signals within complex geological settings and enhances overall flexibility and adaptability.

2.4. Objective function

In the task of seismic sparse spike deconvolution, the insufficiency of model prior information makes it difficult to directly apply the traditional deep learning end-to-end objective function. This study introduces a self-supervised objective function to overcome this limitation. This objective function skillfully incorporates geophysical features, enabling full utilization of the inherent structure of input data for model optimization, while significantly enhancing the interpretability of deep learning models for geophysical applications. Specifically, the objective function is defined as **Equation 8**:

$$L = A \cdot \frac{1}{2} \|D \cdot x - y\|_2^2 + B \cdot \|x\|_1 \tag{8}$$

In **Equation 8**, A and B are coefficients used to balance the data fitting term and the sparse regularization term. D is a dictionary composed of seismic wavelets and is represented by a Toeplitz-type convolution matrix. The reflection coefficient result output by the model is denoted by x, and the input seismic record is denoted by y. This objective function ensures the consistency between the model output and the input data by minimizing the data fitting term $\|D \cdot x - y\|_2^2$, and at the same time uses the sparse regularization term $\|x\|_1$ to promote the model to output sparse reflection coefficients.

Compared with supervised training of Ada-LISTA, the proposed self-supervised objective improves applicability when labeled data or strong priors are unavailable, and can effectively capture the sparse features in seismic signals. This enables us to optimize the effect of sparse spike deconvolution without relying on a large amount of labeled data, thereby improving the seismic resolution.

2.5. Dataset construction and model optimization

To verify the performance of the model, this study conducted experiments using both synthetic data and actual seismic data. The synthetic dataset was produced by convolving Ricker wavelets with randomly generated reflection coefficient sequences. All data were normalized to facilitate parameter learning, optimization, and performance evaluation of the model. The actual seismic data were obtained from a seismic profile of an oilfield in the Bohai Bay Basin, China. For the field data, the statistical wavelet was extracted from the seismic profile based on the Wiener–Levinson process, adopting the autocorrelation method. The amplitude spectrum was derived from the autocorrelation of seismic traces, and a minimum phase spectrum was specified as the input parameter. After normalizing the extracted wavelet by its maximum absolute amplitude, it was used to construct the Toeplitz convolution matrix, forming the wavelet dictionary D for inversion. The seismic data in this area are of poor quality, reflecting the complex geological structure of the oilfield and providing a realistic scenario for evaluating model performance. Seismic record reconstruction was performed to effectively enhance the resolution of actual seismic data, thereby revealing the details of underground geological structures more clearly.

In the model optimization stage, this study employed the Adam optimization algorithm with a learning rate of 1×10^{-9} and a batch size of 8, leveraging its stability and fast convergence capability to update model parameters. To balance inversion accuracy and computational efficiency, the maximum number of iterations was set to 400, with an early stopping mechanism incorporated during the iterative process, where the iteration terminates when the Euclidean norm of the difference between successive

estimates is <0.1 for two consecutive iterations, avoiding redundant computations while ensuring inversion stability. To enhance the generalization capacity, an L_1 regularization term with a strength of 0.01 was introduced to constrain the complexity of model parameters and reduce the risk of overfitting. Meanwhile, an adaptive amplitude adjustment parameter was incorporated to dynamically regulate the amplitude range of model outputs, enabling better adaptation to the amplitude characteristics of different data and improving the model's adaptability to complex geological conditions. To further quantify the deconvolution performance of each method, relative error (Err) was introduced as an evaluation metric, calculated as **Equation 9**:

$$E_{rr} = \frac{\|\hat{r} - r\|}{\|r\|} \tag{9}$$

where $\hat{r}$ denotes the algorithm's deconvolved result, and r represents the actual reflectivity coefficient. A smaller Err value indicates that the deconvolved result is closer to the actual reflectivity coefficient, signifying superior method performance.

3. Results

3.1. Simulation experiments

To evaluate the proposed sparse spike deconvolution method, a simulated seismic dataset was constructed based on the method introduced in **Section 2.5**, and comparative experiments were conducted. The simulated seismic signals were created through the convolution of a zero-phase Ricker wavelet, with a dominant frequency of 40 Hz, and randomly generated reflection coefficients with amplitudes distributed in the interval, thereby spanning both strong and weak reflections. Each trace of the reflection coefficients and seismic records in the final simulated dataset had a duration of 1300 ms, containing

six reflection positions. To facilitate comprehensive feature extraction by the network, a total of 1000 traces of simulated data were generated, and one of them is shown in Figure 4.

The algorithm was used to test the simulated dataset with comparisons to the classical ISTA and LISTA algorithms (Figure 5). Quantitative results showed that the Err of ISTA, LISTA, and the proposed Ada-LISTA was 0.6237, 0.1479, and 0.0422, respectively. While all benchmark methods can achieve wavelet compression, ISTA suffers from significant amplitude loss and poor weak reflection recovery due to cumbersome manual parameter tuning. Additionally, although LISTA improved upon ISTA by adopting learnable parameters, our Ada-LISTA further outperformed both via adaptive adjustment to dynamically optimize thresholds and step sizes, thus achieving superior amplitude recovery and weak reflection identification.

3.2. Noise robustness evaluation

To further validate the efficacy of the algorithm, this study tested data with added random noise. Based on the synthetic seismic record shown in Figure 4B, random noise of different intensities was added to obtain three sets of noisy seismic records. The results are shown in Figure 6. These three models correspond to the high signal-to-noise ratio (SNR) theoretical model in Figure 6A, the medium SNR theoretical model in Figure 6B, and the low SNR theoretical model in Figure 6C.

When the SNR was 10 dB, as shown in Figure 7, the Err values for ISTA, LISTA, and the proposed Ada-LISTA were 0.7561, 0.1979, and 0.0526, respectively. When the SNR decreased to 3 dB, as presented in Figure 8, the Err values were 0.7640, 0.2312, and 0.0819 for the three methods. Traditional ISTA showed apparent amplitude attenuation and poor weak reflection recovery, with performance further deteriorating as SNR decreased. LISTA achieved certain improvements over ISTA by adopting learnable
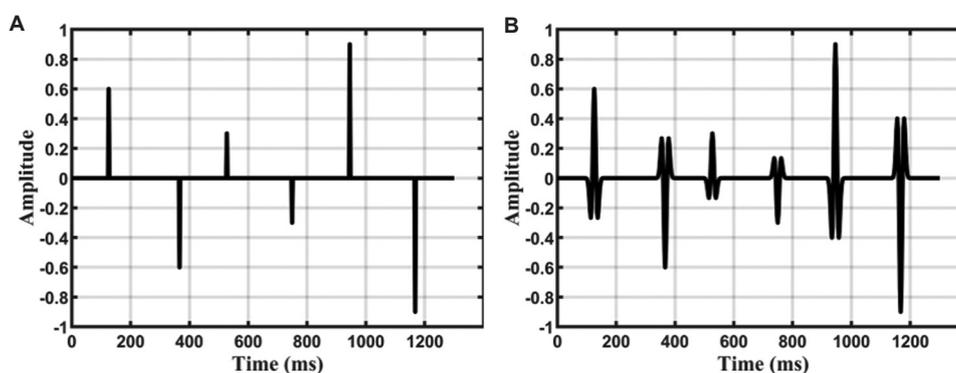

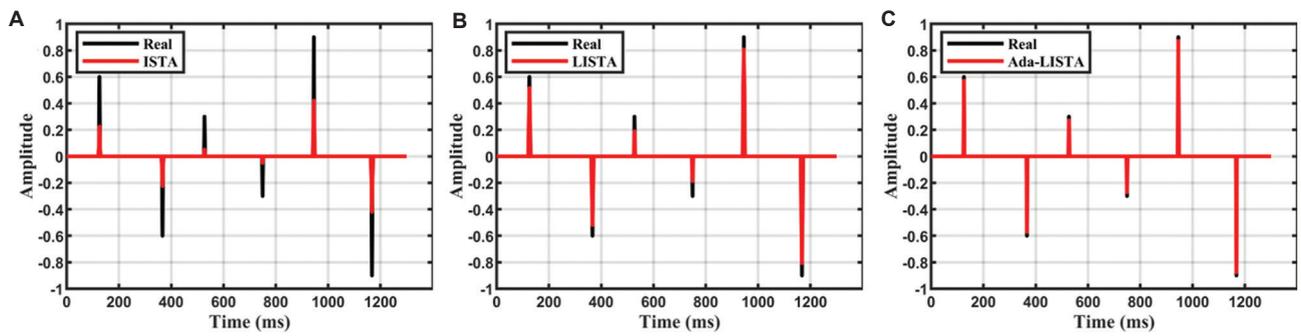**Figure 4.** Theoretical model. (A) Reflection coefficient. (B) Synthetic seismogram.

Figure 5. Deconvolution results on noise-free simulated data. (A) Iterative shrinkage-thresholding algorithm (ISTA). (B) Learned ISTA (LISTA). (C) Adaptive LISTA.
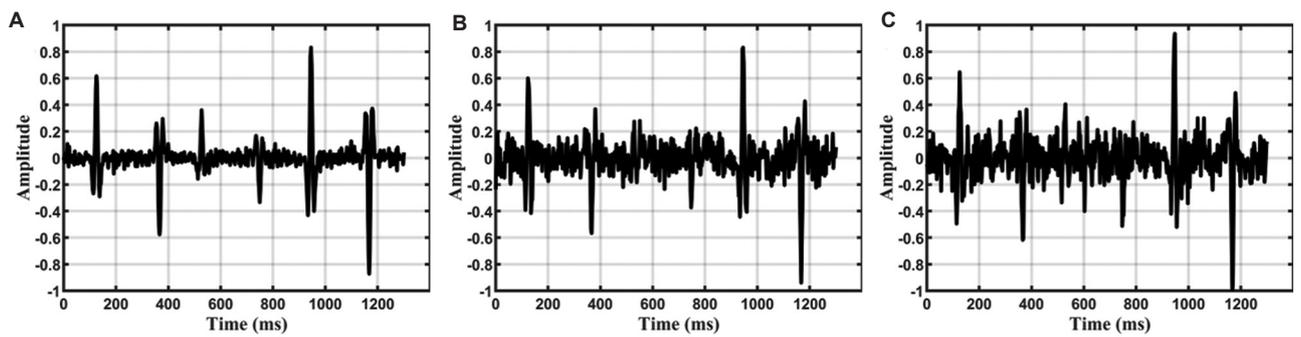

Figure 6. Noisy theoretical model. Signal-to-noise ratio of (A) 10 dB, (B) 3 dB, and (C) 1 dB.
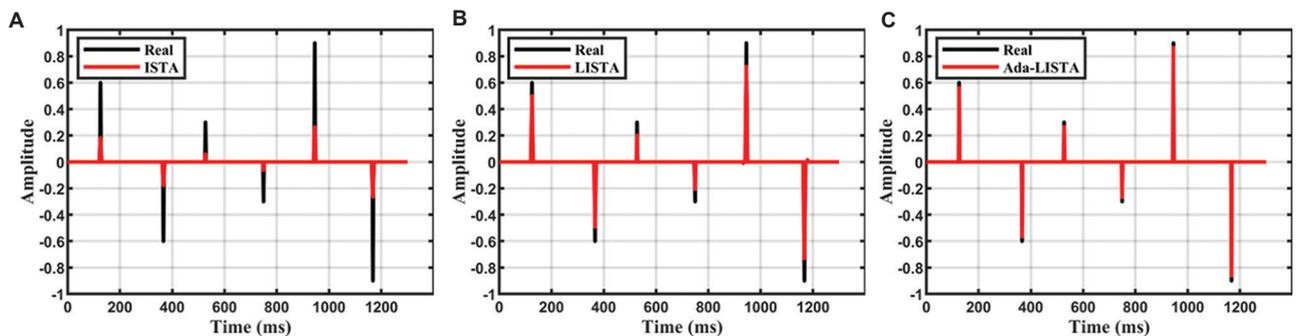

Figure 7. Deconvolution results at a signal-to-noise ratio of 10 dB. (A) Iterative shrinkage-thresholding algorithm (ISTA). (B) Learned ISTA (LISTA). (C) Adaptive LISTA.

Figure 8. Deconvolution results at a signal-to-noise ratio of 3 dB. (A) Iterative shrinkage-thresholding algorithm (ISTA). (B) Learned ISTA (LISTA). (C) Adaptive LISTA.

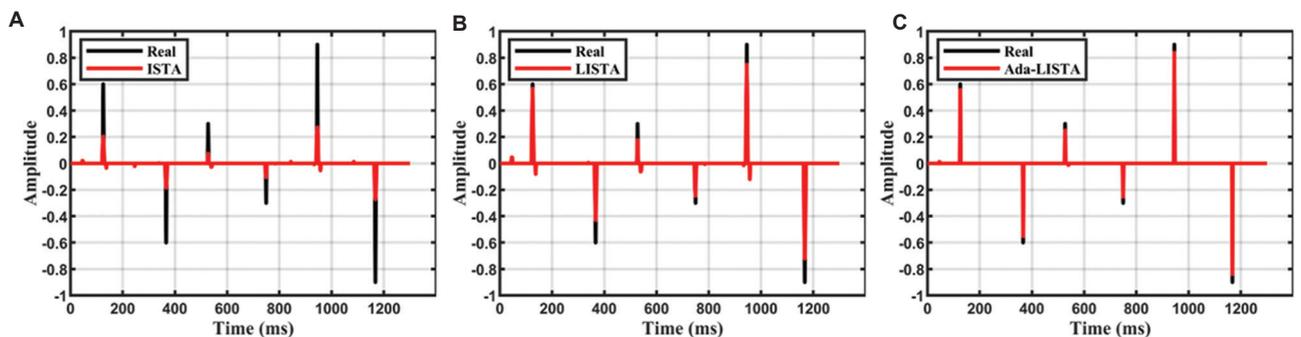parameters, whereas Ada-LISTA demonstrated superior noise robustness, realizing better amplitude recovery and maintaining higher accuracy in weak reflection coefficient recovery compared to both benchmarks.

When the SNR was as low as 1 dB, as depicted in Figure 9, the Err of ISTA, LISTA, and the proposed Ada-LISTA were 0.8007, 0.3582, and 0.1851, respectively. The deconvolution performance of the traditional ISTA algorithm degraded significantly. Amplitude attenuation was prominent, and weak reflection coefficients can hardly be accurately recovered. While LISTA achieved certain improvements over ISTA, it still struggled with severe noise interference. In comparison, although the method proposed in this study was affected by noise interference, its deconvolution results can still maintain a certain reliability under extremely low SNR conditions. It also outperformed the traditional ISTA and LISTA algorithms in both amplitude recovery effect and weak reflection coefficient identification ability. These results indicate that the method proposed in this study

has stronger robustness and reflection coefficient recovery ability when processing low SNR data.

3.3. Application of real seismic data

Seismic data from the lower member of the Minghuazhen Formation in an oilfield within the Bohai Bay Basin, China, were chosen to evaluate the algorithm's applicability. The data has a sampling interval of 2 ms. Within the work area, structural undulations were small, faults were relatively well-developed, and strata were well-developed. The original seismic data of the target interval were of poor quality, with poor continuity of event axes, vague reflection interfaces, and low overall resolution. A local seismic profile of this target interval is shown in Figure 10, which did not meet the requirements for fine reservoir characterization and was suitable as actual data for verifying the effectiveness of the algorithm.

After processing with the traditional ISTA algorithm, the results in Figure 11A show that the continuity of
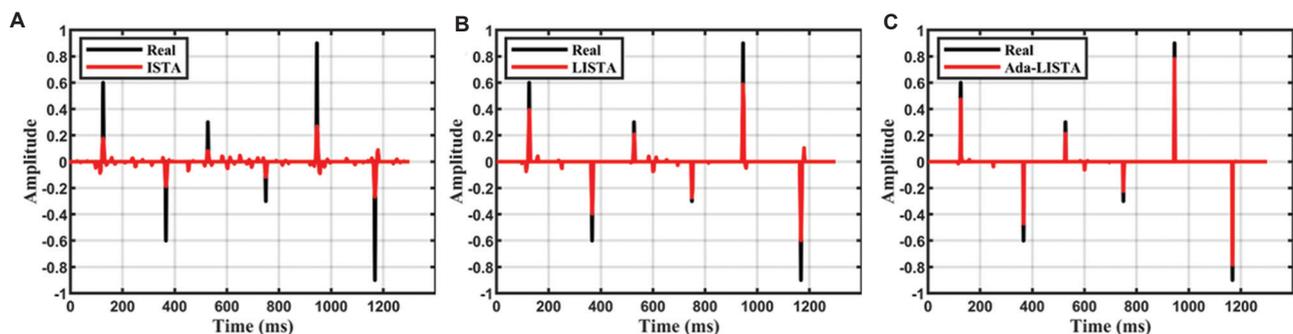

Figure 9. Deconvolution results at a signal-to-noise ratio of 1 dB. (A) Iterative shrinkage-thresholding algorithm (ISTA). (B) Learned ISTA (LISTA). (C) Adaptive LISTA.
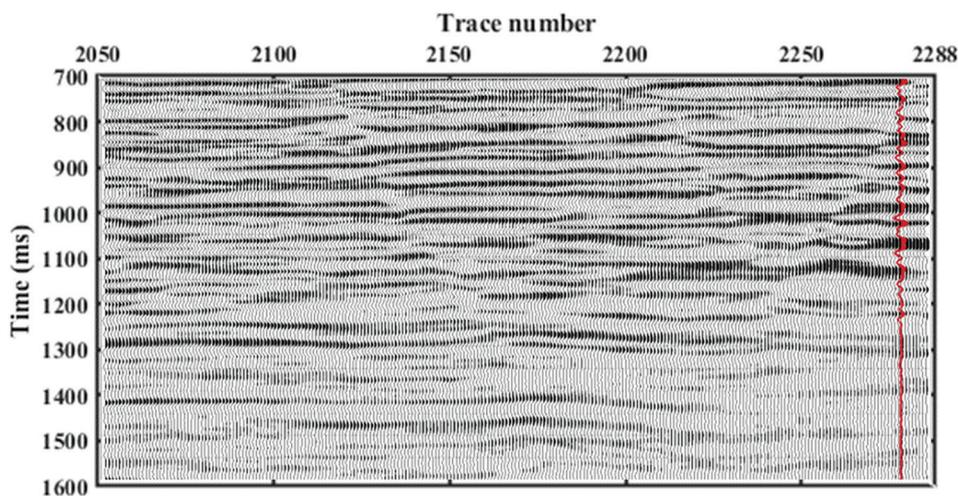

Figure 10. Field seismic data of the Minghuazhen Formation in an oilfield within the Bohai Bay Basin, China.
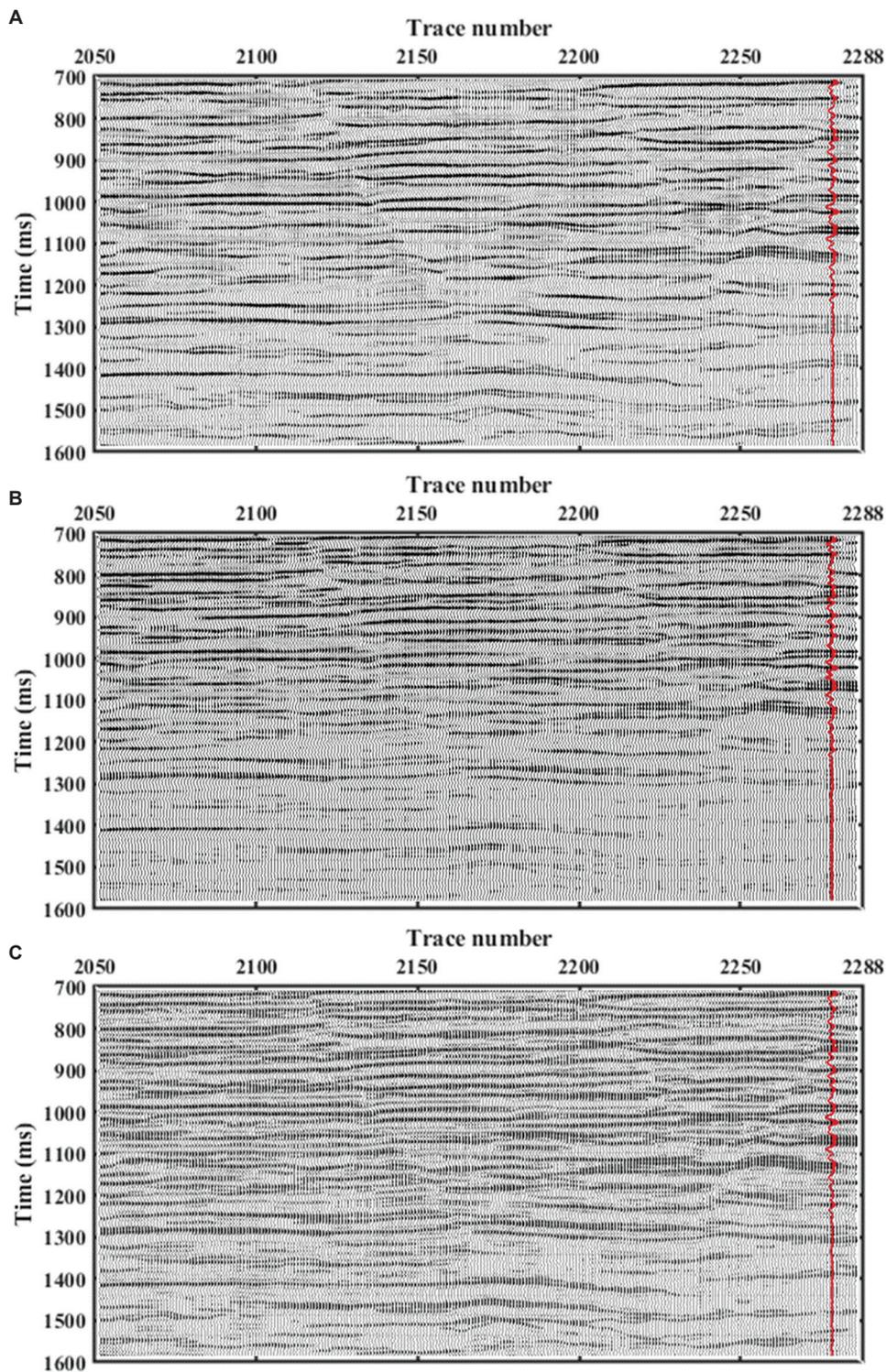
Figure 11. Deconvolution results of the Minghuazhen Formation in an oilfield within the Bohai Bay Basin, China. (A) Iterative shrinkage-thresholding algorithm (ISTA). (B) Learned ISTA (LISTA). (C) Adaptive LISTA.

seismic events in some regions of the seismic profile improved, with enhancements in the clarity of certain reflection interfaces. Compared with the original profile, the resolution increased, but the overall characterization

of details remained limited. Seismic events in some areas were still blurred, and the recovery of weak reflection signals was unsatisfactory. While LISTA outperformed ISTA in event continuity (Figure 11B), it still lacked sufficient weak reflection recovery due to its fixed dictionary. After processing with our method, the results in Figure 11C revealed a notable increase in the quantity of seismic events in the seismic profile. The distribution of interfaces was denser and more continuous. The clarity and detail characterization of seismic events were notably enhanced. Especially, the initially vague weak reflection zones were effectively strengthened. Reflection interfaces became sharper. Overall interpretability improved, with better agreement with the well log.

These results were further verified by Pearson correlation coefficient calculations. The correlation coefficient for the original profile and the well log was 0.6831, which increased to 0.8103 after ISTA processing and to 0.8369 after LISTA processing. The profile processed using the proposed method achieved the highest correlation with the well log, at 0.8783.

To further compare differences in the characterization of seismic profile details among various methods, a typical area within the aforementioned profile was selected for magnification of local information, as shown in Figure 12.

Comparisons revealed that in the detail area of the original profile, as presented in Figure 12A, the events were interleaved and reflections were blurred. After processing with the traditional ISTA, as shown in Figure 12B, some events were separated to a certain extent, but details remained limited. Although LISTA resolved more events than ISTA, the results in Figure 12C show that it failed to adequately distinguish weak reflections and thin layers. In contrast, after processing with our method, as depicted in Figure 12D, the events were continuous and detailed, and the thin-layer structures and weak reflection events were expressed more clearly. Specifically, weak reflection coefficients (marked by red arrows in Figure 12) were distinctly resolved, while the fidelity of the proposed method (indicated by blue arrows in Figure 12) was validated by the well-preserved strong reflections inherent to the original data. This aligns with changes in the overall profile and significantly enhances the identifiability of small-scale structures and thin interbeds within reservoirs.

The results of spectral analysis in Figure 13 indicate that, compared with the original seismic records and the traditional ISTA and LISTA methods, the method proposed in this study showed a gentler amplitude attenuation in the medium and high-frequency bands. The dominant frequency was progressively increased from 37.5 Hz for the original data to 47.5 Hz after ISTA, 52.5 Hz

after LISTA, and 62.5 Hz after Ada-LISTA. Moreover, the effective bandwidth measured at −3 dB broadened from 42 Hz for the original records to 47 Hz after ISTA, 52.5 Hz after LISTA, and 60.5 Hz after Ada-LISTA. These quantitative improvements confirm that the proposed method significantly widened the effective frequency band and increased the dominant frequency, leading to a noticeable improvement in overall resolution. It also exhibited a stronger ability to recover high-frequency and weak signals.

To further validate the generalization capability of the method for more complex geological structures, this study tested it on actual seismic data from another work area. This area exhibited more intricate geology with significant lateral variations in stratigraphy. The field seismic data were characterized by a low SNR and poor resolution, featuring a dominant frequency of only 24 Hz and a narrow effective bandwidth. Consequently, this new dataset provided a more suitable test for evaluating the algorithm's adaptability and robustness under challenging low SNR and low-resolution conditions.

Figure 14 displays the field seismic data, which exhibited poor continuity of the event axes and vague reflection interfaces. These data were processed using the traditional ISTA, LISTA, and the proposed Ada-LISTA methods, with the results presented in Figure 15.

A comparison revealed that the ISTA-processed result (Figure 15A) only partially improved the continuity of the event axes, with a correlation coefficient of 0.5768 compared to 0.5055 for the field seismic data. Its ability to enhance weak reflections was limited, and the overall profile remained blurred. The LISTA-processed result (Figure 15B) showed an improvement over ISTA, yielding clearer event axes and achieving a higher correlation of 0.7550. However, its performance was constrained by a fixed dictionary, which limited its adaptability to complex geological structures. In contrast, the profile processed by the proposed Ada-LISTA method (Figure 15C) demonstrated superior performance, attaining the highest correlation coefficient of 0.8053. It exhibited significantly enhanced event continuity, successfully recovered more weak reflection events, presented sharper reflection interfaces, and ultimately revealed richer geological details.

To further compare the differences in detail rendering among the various methods, a typical region within the profile was selected for local magnification, as shown in Figure 16. The local details in the field seismic data (Figure 16A) exhibited cross-cutting events and disordered reflections. Although the ISTA-processed result (Figure 16B) demonstrated some separation effect, the details remained relatively coarse. The LISTA
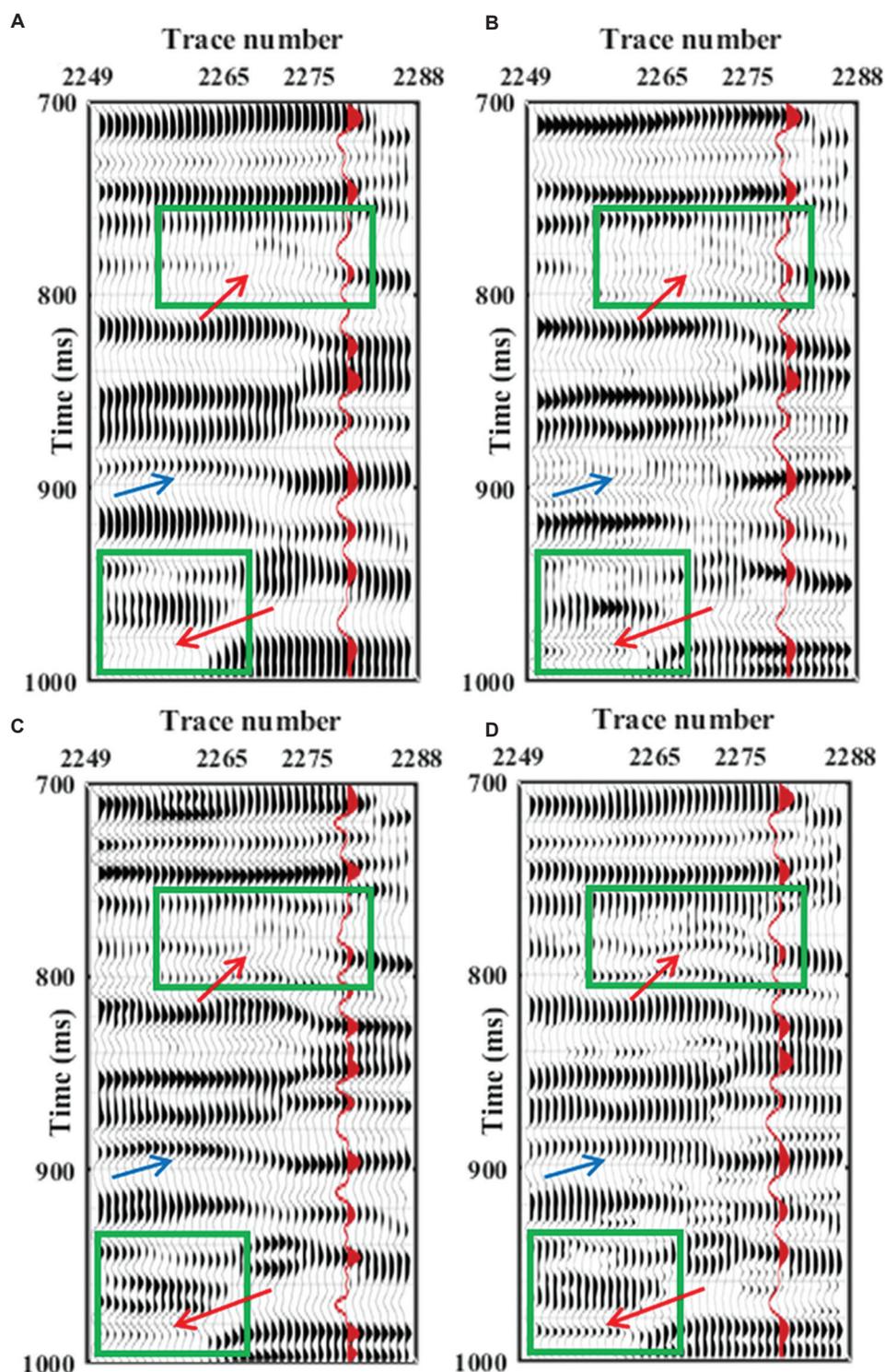
Figure 12. Amplified view of local details from the deconvolution results of the Minghuazhen Formation in an oilfield within the Bohai Bay Basin, China. (A) Field seismic data. (B) Iterative shrinkage-thresholding algorithm (ISTA). (C) Learned ISTA (LISTA). (D) Adaptive LISTA.

result (Figure 16C) resolved more seismic events but exhibited limited ability to distinguish thin interlayers and weak reflections. In contrast, the result from the method proposed in this study (Figure 16D) presented a continuous, clear arrangement of seismic events. Both thin-layer structures and weak reflection events were

clearly depicted, while strong reflection signals maintained fidelity consistent with the field data.

The spectral analysis results in Figure 17 further validated the significant effectiveness of this method in expanding the frequency band and enhancing the dominant frequency. The dominant frequency progressively increased from 24 Hz for the original data to 38 Hz after ISTA, 52 Hz after LISTA, and 58 Hz after Ada-LISTA. Moreover, the effective bandwidth measured at −3 dB broadened from 17.5 Hz for the original records to 29.5 Hz after ISTA, 54 Hz after LISTA, and 57 Hz after Ada-LISTA. This demonstrates that the method proposed in this paper can effectively broaden the effective frequency band, increase the dominant frequency, and significantly improve profile resolution and
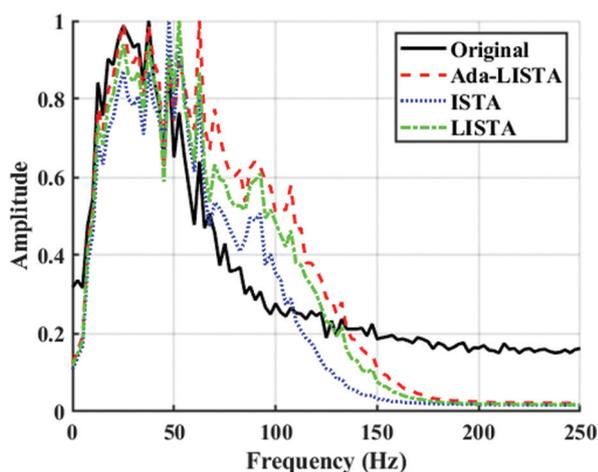
geological detail recognition capability even in work areas with more complex geological conditions.

The experimental results above demonstrate that the proposed sparse pulse deconvolution method, based on Ada-LISTA and a physics-driven self-supervised objective function, exhibited excellent generalization capability and stability across diverse geological backgrounds and resolution conditions. It effectively restored weak reflection signals and enhanced seismic data resolution, thereby possessing significant practical application value.

4. Discussion

This study developed a sparse spike deconvolution method based on the Ada-LISTA network architecture. The method effectively improved the shortcomings of the traditional ISTA algorithm in recovering weak reflection coefficients and notably boosted the algorithm's overall processing performance by introducing a self-supervised objective function and integrating an adaptive learning mechanism, based on the Ada-LISTA architecture. It dynamically adjusts threshold and step size parameters through an adaptive learning mechanism, thus effectively overcoming the deficiencies of traditional ISTA in recovering weak reflection coefficients. Meanwhile, in response to the actual needs of seismic data processing, the self-supervised objective function was incorporated into the model optimization process, enabling it to better express and recover weak reflection signals under complex geological conditions without the need for labeled data. Compared with LISTA and its variants, this method uses the dictionary as the network input, further enhancing the model's adaptability to different scenarios. It performed exceptionally well in processing weak reflection signals, demonstrating stronger generalization performance and practical effects.

Figure 13. Spectrum analysis of the Minghuazhen Formation in an oilfield within the Bohai Bay Basin, China

Abbreviations: Ada: Adaptive; ISTA: Iterative shrinkage-thresholding algorithm; L: Learned.
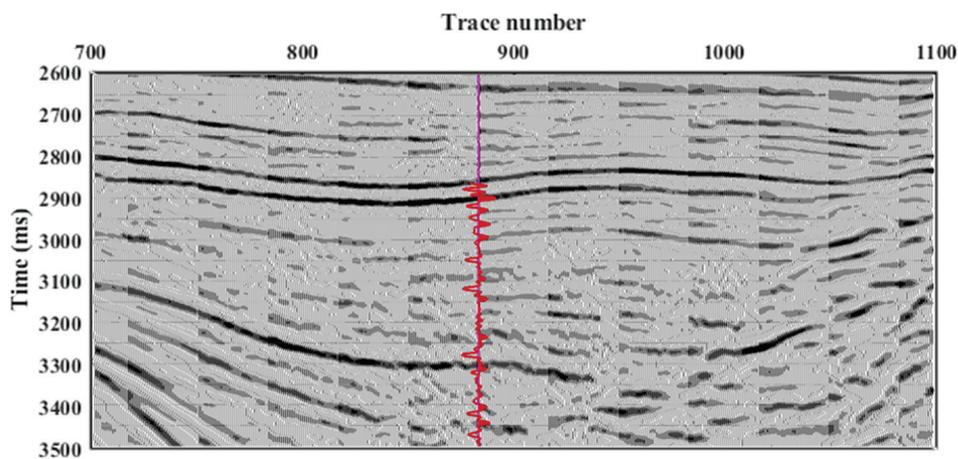

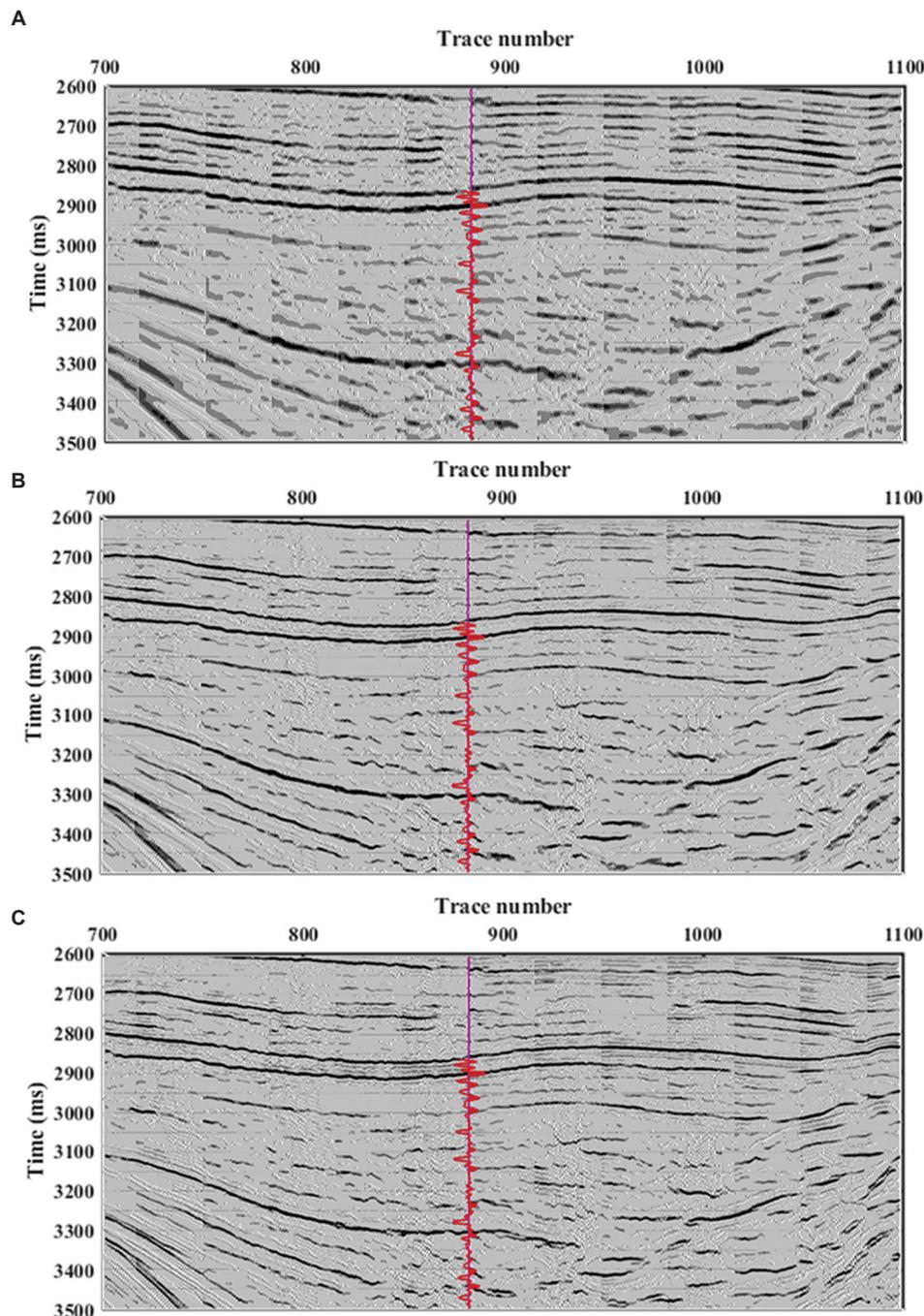**Figure 14.** Field seismic data of the second work area.

Figure 15. Deconvolution results of the second work area. (A) Iterative shrinkage-thresholding algorithm (ISTA). (B) Learned ISTA (LISTA). (C) Adaptive LISTA.

To evaluate the performance of the proposed approach, comparative experiments were conducted against traditional ISTA and LISTA. The results demonstrated that Ada-LISTA, which incorporated a self-supervised learning mechanism, exhibited superiority across multiple testing scenarios. In tests with simulated seismic data, this method not only enhanced the recovery accuracy of reflection coefficients but also performed excellently in thin layer identification and weak reflection signal enhancement. In noise resistance experiments, it can still effectively extract reflection coefficients even under low SNR conditions, showing stronger robustness and stability.
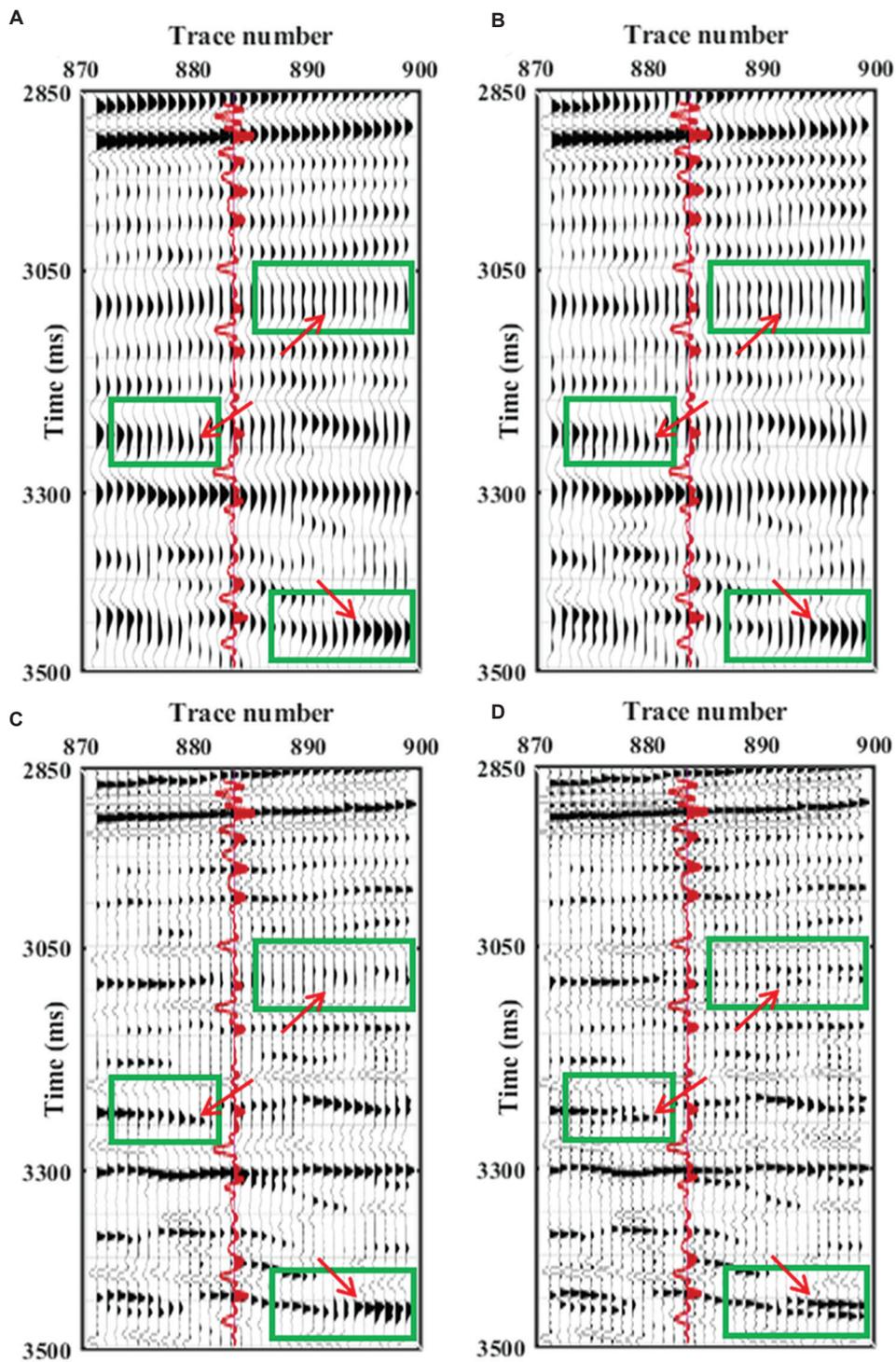
Figure 16. Amplified view of local details from the deconvolution results of the second work area. (A) Field seismic data. (B) Iterative shrinkage-thresholding algorithm (ISTA). (C) Learned ISTA (LISTA). (D) Adaptive LISTA.

These experimental findings robustly demonstrated the efficacy of the proposed approach when applied to complex seismic data.

The proposed method exhibited significant advantages in recovering weak reflection coefficients. Compared with the inversion with elastic-net regularization,[42] which relies

Figure 17. Spectrum analysis of the second work area
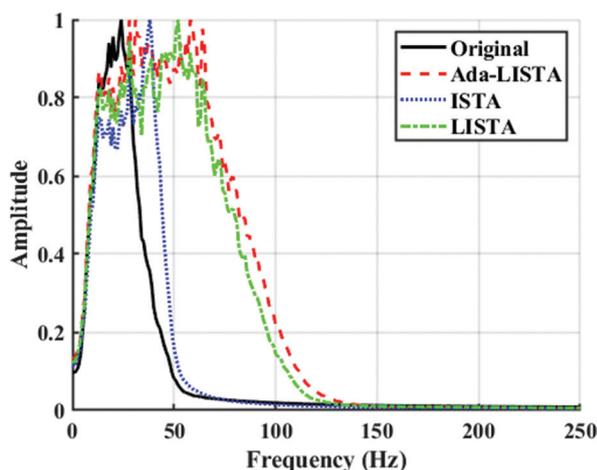Abbreviations: Ada: Adaptive; ISTA: Iterative shrinkage-thresholding algorithm; L: Learned.

heavily on prior model constraints during the recovery of weak reflection signals, the method achieved accurate recovery of weak reflection coefficients without labeled data through a self-supervised objective function and an adaptive dictionary update strategy. Basis pursuit denoising in the joint time–frequency domain[43] improves time–frequency resolution via basis pursuit denoising technology, but suffers from high parameter sensitivity. In contrast, our proposed method adopted an adaptive learning mechanism to realize dynamic parameter adjustment, which effectively enhanced the ability to extract weak reflection signals under different geological scenarios. The seismic wavelet shape-oriented reflectivity inversion[44] method performs optimization based on prior assumptions of waveform shapes, and its performance is easily constrained. In contrast, the proposed approach integrated a deep-learning-based framework with geophysical prior knowledge and further improved recovery accuracy and adaptability through optimized objective function design. Extragradient-based LISTA[24] improves model performance through residual structures and modified threshold functions, but still has limitations under complex geological conditions. Our proposed method further integrated residual structures with deep learning methods, fully exploited geophysical prior information, and significantly enhanced the identification and recovery effects of weak reflection signals.

Application of the proposed method to real seismic data demonstrated that Ada-LISTA, combined with a self-supervised learning mechanism, significantly improved the resolution of seismic sections, thereby verifying its practical effectiveness. However, the method still has several limitations in practical applications. Wavelet phase

shift can introduce non-negligible errors in deconvolution accuracy, especially when the zero-phase assumption deviates from actual conditions, leading to waveform distortion. To mitigate such errors and waveform distortion, Chen *et al.*[45] proposed that envelope-based sparse constraints can enhance wavelet stability, and also demonstrated that full-band data reconstruction is effective in addressing wavelet instability during inversion.[46]

The current noise robustness evaluation was limited to Gaussian random noise, which differs from real seismic scenarios where coherent noise and non-stationary noise are prevalent. These complex noise types can mask weak reflection signals and degrade inversion consistency more severely than Gaussian noise. Meanwhile, the balance coefficients A and B and adaptive parameters in the self-supervised objective function have demonstrated favorable performance for the actual seismic data used in this study. They may show reduced adaptability when applied to data with distinct geological backgrounds or signal characteristics due to the variability of subsurface structures. In addition, the multi-level iteration of Ada-LISTA requires adaptive updates of thresholds, step sizes, and weight matrices for each layer, which increases computational complexity for large-scale seismic surveys. Runtime comparison with ISTA and LISTA on the field data showed that Ada-LISTA takes approximately 1.5 times longer than LISTA due to adaptive parameter learning. High sampling rates can further amplify this burden, potentially limiting the method's practicality in time-sensitive large field projects. This runtime increase is manageable for medium-scale surveys but necessitates targeted optimization for field-scale applications.

Although the sparse spike deconvolution method constructed based on Ada-LISTA has achieved significant progress in several aspects, the model relies on the integrity and variety of the input datasets. Its computational efficiency may be affected when processing extremely high sampling rates or extremely complex geological structures. In this study, a self-supervised objective function was introduced into the Ada-LISTA framework, enabling the model to achieve adaptive optimization without labeled data and effectively expanding the application scope.

To address these limitations, future research should focus on multiple aspects. Researchers can integrate more sophisticated deep learning frameworks to enhance processing performance and computational efficiency. Adaptive parameter-tuning strategies, tailored to diverse data scenarios, can be explored to improve the model's generalization capability. Additionally, multi-task learning and transfer learning can be employed to increase the model's adaptability to different geological conditions. To

bolster robustness against various types of seismic noise, noise-specific suppression strategies can be integrated with adaptive learning mechanisms. Furthermore, lightweight network design and iterative pruning can be adopted to balance inversion performance with computational efficiency while maintaining high accuracy. Collectively, these advancements aim to address the challenges posed by the complexity and diversity of seismic data, which demand superior generalization from the model.

5. Conclusion

An enhanced seismic sparse spike deconvolution method was developed by integrating a self-supervised learning mechanism into the Ada-LISTA architecture. This method dynamically optimized threshold and step size parameters while refining the objective function by incorporating geophysical prior knowledge. It not only markedly strengthened the capability to recover weak reflection signals but also further elevated the model's interpretability and adaptability. Simultaneously, by utilizing the dictionary as input data, the model's adaptability to diverse geological scenarios was effectively enhanced, successfully surmounting the limitations of traditional methods when addressing complex geological conditions. Applied to real seismic data from the Bohai Bay Basin, China, this approach demonstrated significant advantages in enhancing the resolution of seismic profiles. It effectively remedied the deficiencies of the traditional ISTA algorithm in the recovery of weak reflection signals, offering reliable technical support for the detailed interpretation of complex geological bodies.

Acknowledgments

None.

Funding

Conflict of interest

The authors declare they have no competing interests.

Author contributions

Conceptualization: Shunhao Hu, Shulin Pan
Formal analysis: Ziyu Qin
Investigation: Shunhao Hu, Shulin Pan, Yaojie Chen
Methodology: Yinghe Wu
Validation: Shulin Pan
Visualization: Shunhao Hu, Yaojie Chen
Writing–original draft: Shunhao Hu
Writing–review & editing: Shunhao Hu, Shulin Pan, Yinghe Wu

Availability of data

The data are available from the corresponding author on reasonable request.

References

1. Pan S, Yan K, Lan H, Badal J, Qin Z. Adaptive step-size fast iterative shrinkage-thresholding algorithm and sparse-spike deconvolution. *Comput Geosci*. 2020;134:104343.

 doi: 10.1016/j.cageo.2019.104343

2. Levy S, Fullagar PK. Reconstruction of a sparse spike train from a portion of its spectrum and application to high-resolution deconvolution. *Geophysics*. 1981;46(9):1235-1243.

 doi: 10.1190/1.1441261

3. Lavielle M. 2-D bayesian deconvolution. *Geophysics*. 1991;56(12):2008-2018.

 doi: 10.1190/1.1443013

4. Walden AT, Hosken JWJ. An investigation of the spectral properties of primary reflection coefficients. *Geophys Prospect*. 1985;33(3):400-435.

 doi: 10.1111/j.1365-2478.1985.tb00443.x

5. Walden AT. Non-gaussian reflectivity, entropy, and deconvolution. *Geophysics*. 1985;50(12):2862.

 doi: 10.1190/1.1441905

6. Symes WW. The seismic reflection inverse problem. *Inverse Probl*. 2009;25(12):123008.

 doi: 10.1088/0266-5611/25/12/123008

7. Chen SS, Donoho DL, Saunders MA. Atomic decomposition by basis pursuit. *SIAM J Sci Comput*. 1998;20(1):33-61.

 doi: 10.1137/s1064827596304010

8. Mallat SG, Zhang Z. Matching pursuits with time-frequency dictionaries. *IEEE Trans Signal Process*. 1993;41(12):3397-3415.

 doi: 10.1109/78.258082

9. Cai TT, Wang L. Orthogonal matching pursuit for sparse signal recovery with noise. *IEEE Trans Inform Theory*. 2011;57(7):4680-4688.

 doi: 10.1109/tit.2011.2146090

10. Beck A, Teboulle M. A fast iterative shrinkage-thresholding algorithm for linear inverse problems. *SIAM J Imaging Sci*. 2009;2(1):183-202.

 doi: 10.1137/080716542

11. Zhang J, Ghanem B. ISTA-Net: Interpretable Optimization-Inspired Deep Network for Image Compressive Sensing. In: *2018 IEEE/CVF Conference on Computer Vision and Pattern Recognition (CVPR)*. Salt Lake City, UT, USA: IEEE; 2018. p. 1828-1837.

    doi: 10.1109/cvpr.2018.00196

12. Schnoor E, Behboodi A, Rauhut H. Generalization error bounds for iterative recovery algorithms unfolded as neural networks. *Inf Inference*. 2023;12(3):2267-2299.

    doi: 10.1093/imaiai/iaad023

13. Pan S, Yan K, Lan H, Badal J, Qin Z. A sparse spike deconvolution algorithm based on a recurrent neural network and the iterative shrinkage-thresholding algorithm. *Energies*. 2020;13(12):3074.

    doi: 10.3390/en13123074

14. Ito D, Takabe S, Wadayama T. Trainable ISTA for sparse signal recovery. *IEEE Trans Signal Process*. 2019;67(12):3113-3125.

    doi: 10.1109/tsp.2019.2912879

15. Hinton GE, Salakhutdinov RR. Reducing the dimensionality of data with neural networks. *Science*. 2006;313(5786):504-507.

    doi: 10.1126/science.1127647

16. Ranzato M, Boureau YL, LeCun Y. Sparse Feature Learning for Deep Belief Networks. In: Platt J, Koller D, Singer Y, Roweis S, editors. *Proceedings of the 21st Annual Conference on Neural Information Processing Systems(NIPS 2007)*. Vancouver, BC, Canada: Neural Information Processing Systems; 2007. p. 1185-1192.

17. Bengio Y, Lamblin P, Popovici D, Larochelle H. Greedy Layer-Wise Training of Deep Networks. In: Schölkopf B, Platt J, Hoffman T, editors. *Proceedings of the 20th Annual Conference on Neural Information Processing Systems(NIPS 2006)*. Vancouver, BC, Canada: Neural Information Processing Systems Foundation; 2006. p. 153-60.

18. Chai X, Tang G, Lin K, *et al*. Deep learning for multitrace sparse-spike deconvolution. *Geophysics*. 2021;86(3):V207-V218.

    doi: 10.1190/geo2020-0342.1

19. Gregor K, LeCun Y. Learning Fast Approximations of Sparse Coding. In: Furnkranz J, Joachims T, editors. *Proceedings of the 27th International Conference on Machine Learning*. Haifa, Israel; 2010. p. 399-406.

20. Liu J, Chen X, Wang Z, Yin W. Alista: Analytic Weights are as Good as Learned Weights in LISTA. In: *Proceedings of the 7th International Conference on Learning Representations (ICLR 2019)*. New Orleans, LA, United States: International Conference on Learning Representations (ICLR); 2019.

21. Wu K, Guo Y, Li Z, Zhang C. Sparse Coding with Gated Learned ISTA. In: *Proceedings of the 8th International Conference on Learning Representations (ICLR 2020)*. Addis Ababa, Ethiopia: International Conference on Learning Representations (ICLR); 2020.

22. Zheng Z, Dai W, Xue D, Li C, Zou J, Xiong H. Hybrid ISTA: Unfolding ISTA with convergence guarantees using free-form deep neural networks. *IEEE Trans Pattern Anal Mach Intell*. 2022;45(3):3226-3244.

    doi: 10.1109/tpami.2022.3172214

23. Ablin P, Moreau T, Massias M, Gramfort A. Learning Step Sizes for Unfolded Sparse Coding. In: Wallach H, Larochelle H, Beygelzimer A, D'Alché-Buc F, Fox E, Garnett R, editors. *Proceedings of the 33rd Annual Conference on Neural Information Processing Systems (NIPS 2019)*. Vancouver, BC, Canada: Neural Information Processing Systems Foundation; 2019.

24. Li Y, Kong L, Shang F, Liu Y, Liu H, Lin Z. Learned extragradient ISTA with interpretable residual structures for sparse coding. *Proc AAAI Conf Artif Intell*. 2021;35(10):8501-8509.

    doi: 10.1609/aaai.v35i10.17032

25. Kim D, Park D. Element-wise adaptive thresholds for learned iterative shrinkage thresholding algorithms. *IEEE Access*. 2020;8:45874-45886.

    doi: 10.1109/access.2020.2978237

26. Liang W, Liu J, Zhu J. Improved analytic learned iterative shrinkage thresholding algorithm and its application to tomographic synthetic aperture radar building object height inversion. *Mathematics*. 2024;12(10):1464.

    doi: 10.3390/math12101464

27. Chen X, Wang Z, Liu J, Yin W. Theoretical Linear Convergence of Unfolded ISTA and its Practical Weights and Thresholds. In: Bengio S, Wallach H, Larochelle H, Grauman K, Cesa-Bianchi N, Garnett R, editors. *Proceedings of the 32nd Conference on Neural Information Processing Systems*. Montreal, QC, Canada: Neural Information Processing Systems Foundation; 2018. p. 9061-9071.

28. Wang M, Zhang Z, Qiu X, Gao S, Wang Y. ATASI-Net: An efficient sparse reconstruction network for tomographic SAR imaging with adaptive threshold. *IEEE Trans Geosci Remote Sens*. 2023;61:1-18.

    doi: 10.1109/tgrs.2023.3268132

29. Aberdam A, Golts A, Elad M. Ada-LISTA: Learned solvers adaptive to varying models. *IEEE Trans Pattern Anal Mach Intell*. 2022;44(12):9222-9235.

    doi: 10.1109/tpami.2021.3125041

30. Abd Rahman AS, Elsheikh AH, Jaya MS. A deep semi-supervised learning approach for seismic reflectivity inversion. *IEEE Trans Geosci Remote Sens*. 2024;62:5927714.

    doi: 10.1109/tgrs.2024.3401768

31. Alfarraj M, AlRegib G. Semisupervised sequence modeling for elastic impedance inversion. *Interpretation*. 2019;7(3):SE237-SE249.

doi: 10.1190/int-2018-0250.1

32. Zhao Y, Li Y, Wang S, Yang B. Physical model and super-resolution theory-guided unsupervised deep learning deconvolution for seismic resolution enhancement. *IEEE Trans Geosci Remote Sens*. 2025;63:1-13.

doi: 10.1109/tgrs.2025.3531359

33. Liu B, Jiang P, Wang Q, Ren Y, Yang S, Cohn AG. Physics-driven self-supervised learning system for seismic velocity inversion. *Geophysics*. 2023;88(2):R145-R161.

doi: 10.1190/geo2021-0302.1

34. Zhang J, Sun H, Zhang G, Huang X, Han L. Simultaneous physics and model-guided seismic inversion based on deep learning. *IEEE Trans Geosci Remote Sens*. 2024;62:1-11.

doi: 10.1109/tgrs.2024.3443970

35. Schuster GT, Chen Y, Feng S. Review of physics-informed machine-learning inversion of geophysical data. *Geophysics*. 2024;89(6):T337-T356.

doi: 10.1190/geo2023-0615.1

36. Song C, Lu M, Li Y, *et al*. Spatial pattern learning: Dip structure constraint multi-view convolutional neural network for pre-stacked seismic inversion. *IEEE Trans Geosci Remote Sens*. 2023;61:1-16.

doi: 10.1109/tgrs.2023.3307897

37. Feng W, Liu Y, Li Y, Li H, Wang X. Acoustic impedance prediction using an attention-based dual-branch double-inversion network. *Earth Sci Inform*. 2025;18(1):70.

doi: 10.1007/s12145-024-01548-4

38. Zou B, Wang Y, Chen T, Liang J, Yu G, Hu G. The domain adversarial and spatial fusion semi-supervised seismic impedance inversion. *IEEE Trans Geosci Remote Sens*. 2024;62:1-15.

doi: 10.1109/tgrs.2023.3336392

39. Zhu L, Zhang F, Zhang S, Wu J. Semi-supervised intelligent inversion from prestack seismic attributes guided by geophysical prior knowledge. *J Appl Geophys*. 2025;233:105620.

doi: 10.1016/j.jappgeo.2025.105620

40. Shi Y, Zhang B, Xu J, Wang Y, Jin Z. Joint supervised and semi-supervised seismic velocity model building based on VGU network. *IEEE Trans Geosci Remote Sens*. 2025;63:1-14.

doi: 10.1109/tgrs.2025.3533548

41. Ge Q, Cao H, Yang Z, Yuan S, Song C. Deep-learning-based prestack seismic inversion constrained by AVO attributes. *IEEE Geosci Remote Sens Lett*. 2024;21:1-5.

doi: 10.1109/lgrs.2024.3373197

42. Dai R, Yin C, Peng D. An application of elastic-net regularized linear inverse problem in seismic data inversion. *Appl Sci*. 2023;13(3):1525.

doi: 10.3390/app13031525

43. Zhao X, Wu H, Li X, Peng Z, Li Y. Seismic reflection coefficient inversion using basis pursuit denoising in the joint time-frequency domain. *Energies*. 2020;13(19):5025.

doi: 10.3390/en13195025

44. Chen S, Fu X, Shi Y, Cao S. Seismic wavelet shape-oriented reflectivity inversion method. *J Geophys Eng*. 2024;21(4):1216-1229.

doi: 10.1093/jge/gxae065

45. Chen G, Yang W, Liu Y, Luo J, Jing H. Envelope-based sparse-constrained deconvolution for velocity model building. *IEEE Trans Geosci Remote Sens*. 2022;60:1-13.

doi: 10.1109/tgrs.2021.3063514

46. Chen G, Yang W, Wang H, Zhou H, Huang X. Elastic full waveform inversion based on full-band seismic data reconstructed by dual deconvolution. *IEEE Geosci Remote Sens Lett*. 2022;19:1-5.

doi: 10.1109/lgrs.2022.3178915